PEDIATRIC CARDIOLOGY and CARDIAC SURGERY VOL. 24 NO. 5 (606-614)

原　著

心外膜原基由来細胞を制御するテネイシンCの検討

宮川-富田幸子[1]，杉村　洋子[2]，中西　敏雄[1]，今中-吉田恭子[3]

東京女子医科大学循環器小児科[1]，千葉県こども病院集中治療科[2]，
三重大学大学院医学系研究科修復再生病理学[3]

Key words:
tenascin, coronary, epicardium, cardiac neural crest, development

Tenascin-C May Regulate Behavior of Proepicardium-derived Cells

Sachiko Miyagawa-Tomita,[1] Hiroko Sugimura,[2] Toshio Nakanishi,[1] and Kyoko Imanaka-Yoshida[3]

[1]Department of Pediatric Cardiology, Tokyo Women's Medical University, Tokyo, [2]ICU, Chiba Children's Hospital, Chiba, [3]Pathology and Matrix Biology, Mie University Graduate School of Medicine, Mie, Japan

Background: During cardiogenesis, the epicardium derived from the proepicardium (PE) undergoes epithelial-mesenchymal transformation and migrates into the myocardium. These PE-derived cells differentiate into interstitial fibroblasts, coronary smooth muscle cells, and perivascular fibroblasts. However, the origin of the cells forming the orifices of the coronary vessels remains uncertain. Tenascin-C, an extracellular matrix glycoprotein, often appears associated with cell motility of the neural crest and epithelial-mesenchymal/mesenchymal-epithelial transformation, and can accelerate the migration of various types of cells.
Methods: We made PE quail-chick chimeras, cardiac neural crest (CNC) quail-chick chimeras and CNC-ablated chick embryos. Expression of tenascin-C and distribution of the PE-derived and CNC-derived cells were examined.
Results: The PE-derived cells differentiated into epicardial cells, interstitial fibroblasts, coronary smooth muscle cells and endothelial cells, and endocardial cells. CNC-ablation caused anomalies of coronary orifices. Tenascin-C was expressed in the area where epithelial-mesenchymal transformation of PE-derived cells was taking place and around the orifices of the coronary vessels.
Conclusion: The PE-derived and CNC-derived cells contribute to the formation of the coronary orifices, and tenascin-C may regulate their behavior.

要　旨

背景：発生過程で，心外膜前駆組織(PE)から形成される心外膜は，上皮－間葉転換後，心筋層内に潜り込み，間質線維芽細胞，冠動脈平滑筋細胞と外膜周囲線維芽細胞に分化する．しかし，大動脈基部の冠動脈開口構成細胞の起源は不明である．細胞外基質糖蛋白であるテネイシンCは上皮－間葉/間葉－上皮細胞転換や神経堤細胞などの細胞運動を制御している．
方法：PEウズラ-ニワトリキメラ，心臓神経堤(CNC)ウズラ-ニワトリキメラ，CNC除去ニワトリ胚を作成し，テネイシンC発現とPEおよびCNC由来細胞分布を検討した．
結果：PE由来細胞は，心外膜細胞，間質線維芽細胞，冠動脈平滑筋細胞と内皮細胞，心内膜細胞に分化していた．冠動脈開口部はPEとCNC由来細胞が形成に関与していた．テネイシンCは上皮－間葉転換時と，冠動脈開口形成時に特異的な発現を認めた．
結論：発達心におけるPE由来細胞の分布図を作成した．冠動脈開口部ではPEとCNC由来細胞が形成に関わり，テネイシンCは冠動脈形成で重要な役割を担っていることが示唆された．

はじめに

冠動脈の異常には，後天性および先天性のものがある．川崎病や生活習慣病など後天的要因による病変は，臨床上の大きな問題の一つである．先天的には，左冠動脈肺動脈起始(Bland-White-Garland症候群)などの冠動脈単独で起こる異常や，Fallot四徴症や完全大血管転換に伴う単冠動脈などの先天性心疾患に伴って

平成19年8月20日受付
平成20年5月16日受理

起こる冠動脈異常がある．冠動脈の異常は小児に重篤な病態をひき起こすだけでなく，しばしば成人突然死の原因となる[1]．これら冠動脈の病態を理解するためには，その発生と発達を理解することが必須であるが，冠動脈発生に関する研究が数多く報告されるようになってきたのは最近である[2]．

冠動脈は，発生初期肝の心臓と肝臓の間にできる横中隔間葉組織(septum transversum)から発生する心外膜前駆組織(proepicardium：PE)から派生する．左右両側に形成されたPE原基はやがて左側が消失し，右側だけ残り発育する(ニワトリ3日前半胚Hamburger & Hamilton stage：HH16)か，または両側に形成されたPE原基が中央で融合して一つのPEを形成する[マウス胎齢(E)9.5日胚][3]．カリフラワー状の形態を示すPEはまず心筋後壁に付着してから，心筋全体を直接被って心外膜を完成する(ニワトリ4.5～5日胚HH26，マウス胚E12.5)．心外膜細胞は心筋と心外膜の間で，上皮－間葉転換(epithelial-mesenchymal transformation：EMT)を起こし間葉系細胞となって心筋層内に潜り込む．心筋層内で，このPE由来の間葉系細胞は間質線維芽細胞，冠動脈の平滑筋細胞と外膜周囲の線維芽細胞，房室弁の一部の間葉細胞を形成すると考えられているが，冠動脈の内皮細胞がPE由来細胞かどうかはまだ一致した見解は得られていない[4,5]．さらに網目状の細かい血管叢が大動脈肺動脈周囲に形成され，次第に血管叢が伸びて3つの大動脈弁基部に接続してマルチチャネルを形成する．次第に左右の冠動脈弁基部にのみ収束しておのおの1本の太い血管を形成する．しかし，この冠動脈開口部を構成する細胞がPE由来かどうかまだ結論が出ていない．なぜなら，流出路は心外膜が最後に被う部分であるが，その起源はPEではないことが明らかにされ混乱しているためである[6]．つまり心外膜の起源は2つあり，1つはPEで，もう1つは流出路近位の臓側中胚葉(splanchnic mesoderm)由来の頭側心膜(cepharic pericardium)である．2つの異なった組織から派生する心外膜細胞は，それぞれ形態，遺伝子発現プロファイル，EMT能力に違いがあることが示されている．さらに心臓流出路には心臓神経堤(cardiac neural crest：CNC)細胞が遊走侵入してくるため，大動脈基部に開口する冠動脈構成細胞の起源はいまだ解決に至っていない．

一方，細胞外基質糖タンパクであるテネイシンC(tenascin-C)は，一般に胚発生のような形態形成，成体での癌浸潤，創傷治癒，組織再生の際，特定部位に一時的に発現し，上皮－間葉/間葉－上皮細胞転換や神経堤細胞をはじめ一般に細胞遊走の促進など，細胞の運動制御に関与している．テネイシンCは心臓発生初期に左右に形成される心臓原基の中胚葉に発現し，一般に心筋細胞が分化すると発現が消失するが[7]，発達中の心臓流出路には発現がみられることから心臓神経堤細胞の遊走制御にも関わる可能性が考えられる．

そこでわれわれはPEウズラ-ニワトリキメラ胚，CNCウズラ-ニワトリキメラ胚およびCNC焼灼ニワトリ胚を作成して冠動脈形成でのPE由来細胞，CNC由来細胞について検討し，それぞれの細胞におけるテネイシンCの役割を検討した．その結果，PE由来細胞は心外膜を形成し，ほとんどの冠動脈内皮細胞と中膜平滑筋細胞を派生することが明らかとなった．さらに，冠動脈の大動脈基部開口部の細胞は，PE由来細胞とCNC由来細胞の両方が構成に関与していることが明らかとなった．PE細胞ははじめテネイシンCを産生分泌しているが，心筋に付着するとすぐに消失する[7]．PE由来細胞が心外膜下でEMTを起こすときに再びテネイシンC発現が認められるが，EMTを起こした細胞が心筋層内に遊走する際には発現は消失する．心外膜によって心流出路が最後に被われるころ，冠動脈が大動脈基部に開口する．この部分にはPE由来細胞とCNC由来細胞が遊走するが再びテネイシンC発現が認められる．これらのことよりテネイシンCはEMTを促進し，PE細胞が間葉系細胞に転換するのに必要な因子であることが推測された．また，冠動脈開口部形成時にテネイシンC発現が認められることからテネイシンCは冠動脈が大動脈基部の正しい位置に開口するのを誘導する可能性が考えられた．

材料と方法

1．材料

ニワトリ受精卵[(有)城山鶏園，神奈川]とウズラ受精卵[(株)モトキ，埼玉]をあらかじめ37°C，湿潤した孵卵器で孵卵を開始した．PE移植キメラ，CNC移植キメラともにウズラ胚からニワトリ胚に移植した．PE移植キメラにはPE細胞が心臓に付着する前のHH16胚を用いた．CNC移植キメラにはCNC細胞が遊走する前のHH8～9(体節5～7)胚を用いた．免疫染色には，マウス抗ウズラ細胞核膜特異抗体QCPN(Developmental Studies Hybridoma Bank)，マウス抗ウズラ内皮細胞特異抗体QH1(Developmental Studies Hybridoma Bank)，ウサギ抗テネイシンC抗体[8]，マウス抗CD57(Leu7，HNK1)抗体(Becton Dickinson)を用い，horseradish peroxidase(HRP)標識2次抗体を用いたDAB(diaminobenzidine tetrachloride)染色酵素抗体法あるいはFITC(fluorescein isothiocyanate)標識2次抗体による蛍光抗体法

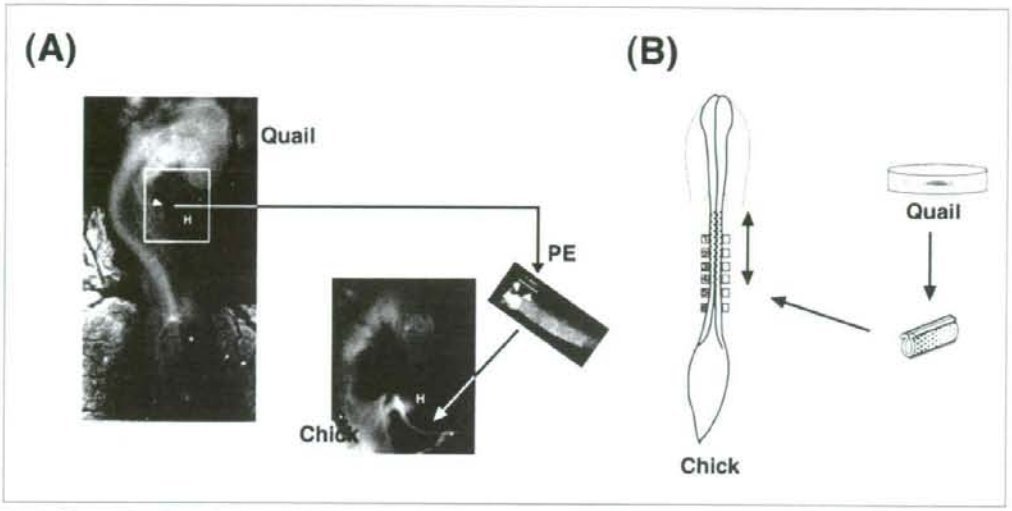

Fig. 1 Preparation of proepicardial (PE) chimera (A) and cardiac neural crest chimera (B) between quail and chick embryos.
The left panel in (A) shows a right lateral view of quail embryo at HH16. Heart (H) and PE tissue (arrowhead) is shown in the boxed area. The right omphalomesenteric vein is opened. A small piece of the shell membrane is pushed forward through the opening. Arrowheads show the PE tissue labeled with fluorescent dye, CM-DiI (right panel). The quail PE tissue with the shell is inserted in the chick-host embryo between the PE tissue and heart (middle panel).
(B) The neural tube (indicated by dotting), which contains the cardiac neural crest before migration, is removed from the chick embryo at HH8-9. The neural tube containing the cardiac neural crest of the HH8-9 quail embryo treated with dispase is transplanted into the ablated chick embryo.

を行った．酵素抗体法染色後にはメチルグリーンあるいはヘマトキシリンで軽く核染色を行った．生体染色には蛍光染色剤CM-DiI（Molecular Probes）あるいはCFDA-SE（Molecular Probes）を用いた．

2. 方法

本実験に供した方法は大きく分けて2つである．1つは，Männer[9]の方法を用いて，HH16のウズラ胚PEをニワトリ胚の同じ部分に移植してPEウズラ-ニワトリキメラを作成した（Fig. 1A）．ウズラ胚をシャーレに取り出し，頭部と尾部を切り離し，一部からだをつけた心臓部分を別シャーレに移した．ウズラPEを実体蛍光顕微鏡下，あるいは正立型蛍光顕微鏡下で追跡確認するために，ウズラPEは蛍光染色剤CM-DiIやCFDA-SEを37℃1時間取り込ませた．卵黄静脈に切れ込みを入れ，長方形に細切した卵殻膜を差し込み，総主静脈－静脈洞間をカットして，このウズラPE全体をウズラ胚から切り離した（Fig. 1A左，右）．HH16のニワトリ胚はあらかじめPEを部分的に切除しておき，同じ部分にウズラPEを移植した．卵殻膜はウズラPEを支えると同時に，ニワトリPE細胞の移動をブロックする役目をする（Fig. 1A中）．この後，孵卵を再び継続し，適当なステージで胚を採取した．採取時，あらかじめ生体染色処理をしてある個体は，蛍光実体顕微鏡でウズラ細胞が付着したかどうか確認し，蛍光細胞が確認できた個体を固定した．一部の個体心はグリセリンで透明化し蛍光実体顕微鏡下で観察した．また，一部のニワトリ胚PE細胞に直接蛍光染色剤を注入して，その細胞系譜を観察した．2つめの方法は，CNC移植ウズラ-ニワトリキメラである（Fig. 1B）．HH8～9のウズラ胚をシャーレに取り出し，dispase処理して脊索を含む神経管（CNC細胞を含む）を取り出した．あらかじめ同じ部分を取り除いたHH8～9のニワトリ胚にウズラCNCを含む神経管を移植して孵卵を継続し，適当なステージで胚を採取した．CNC焼灼除去胚は，ニワトリ胚の神経襞（neural fold）を含むCNCをあらかじめ熱したプローブで取り除き，孵卵を再び継続して適当なステージで胚を採取した．

採取した胚は，4%パラフォルムアルデヒド/PBS（phosphate-buffered saline）に1晩4℃で固定し，翌日PBSで洗浄後，パラフィン包理して連続切片を作成し，免疫組織染色を実施した．生体染色した個体は，

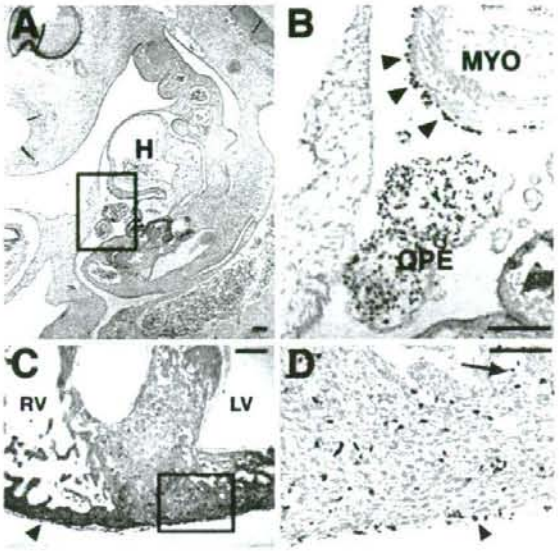

Fig. 2 The distribution of quail cells in proepicardium chimeras.
(A, B) The grafted quail proepicardium attaches to the heart and forms the epicardium (arrowheads) of the HH19 (3 days) chimera embryo. (C, D) Quail-derived cells have migrated into the myocardium and formed the epicardium (arrowhead), endocardium (arrow), and interstitial fibroblasts. The donor-derived cells are detected through immunostaining with anti-quail antibody (QCPN). HH31 (7 days) quail-chick chimeras.
H, Heart; LV, left ventricle; MYO, myocardium; QPE, transplanted quail proepicardium; RV, right ventricle. Scale bar, 100 μm.

正立型蛍光顕微鏡下でこの切片を観察することにより細胞系譜の追跡を実施した.

結　果

1. 心外膜前駆組織由来細胞の時空間的分布

3日胚HH19のPE移植キメラでは，ウズラPE細胞が近位の心筋背側に接着して広がり，心外膜を形成していた(Fig. 2A, B). 4日胚HH24のPEキメラでは，心外膜を形成すると同時に，心外膜と心筋との間でウズラPE細胞がEMTを起こして間葉系細胞に転換し毛細血管を形成し，また一部の細胞は心筋層内に潜り込んでいた. 6.5～7日胚HH30～31のPEキメラで，大動脈基部で冠動脈の開口が認められ，PE細胞は開口部の内皮細胞に分化していた. 心室背側や房室溝でウズラPE細胞の多くがEMTを起こしていた. 5日胚から，多くのPE由来ウズラ細胞が心筋層内に遊走侵入しており，一部は心内膜細胞に寄与していた(Fig. 2C, D). また，血管内皮細胞にも分化し，原始冠動脈網の形成が認められた.

CM-DiIやCFDA-SEで直接，あるいは間接的にPE細胞を蛍光生体染色した観察結果では，PE細胞は心筋表面，心内膜，三尖弁，僧帽弁，左右静脈洞弁に分布していることを確認した.

2. 心外膜前駆組織由来細胞とテネイシンC発現

マウスでは遊走前のPE細胞は，テネイシンCを産生し分泌している[7]. PE由来細胞の時空間的分布を確認後，おもなステージでテネイシンC発現との関係を検討した. 3日胚HH19のPEキメラで，PE細胞は心筋背側に付着遊走し心外膜を形成し始めるがテネイシンC発現は消失していた. 4日胚HH24より心室背側や房室溝の心外膜と心筋間で多数のEMTが認められ毛細血管網が形成され，ここではテネイシンC発現が見られた(Fig. 3A, B). 間葉系細胞となったPE由来ウズラ細胞が心筋層内に侵入する際には，テネイシンCは消失し，心筋層内にも認められなかった. 再びテネイシンC発現が認められるのは大動脈基部への冠動脈開口形成時であった. 6.5～7日胚HH30～31で冠動脈が大動脈に開口するのを確認できた. QCPN抗体染色で，冠動脈内皮がウズラ由来細胞によって形成されていることを確認できたが，QH1抗体染色で，より明らかに開口部内皮細胞がウズラ由来細胞で構成されていることを確認できた(Fig. 3C, D). この開口直後の冠動脈周囲にテネイシンCの沈着が認められた(Fig. 3E).

3. 心臓神経堤細胞の冠動脈開口部への関与

CNC焼灼除去したニワトリ胚を10日HH36で採取し，冠動脈開口部をコントロールと比較した(Fig. 4). コントロール胚73個では，右冠動脈弁基部に1個と，

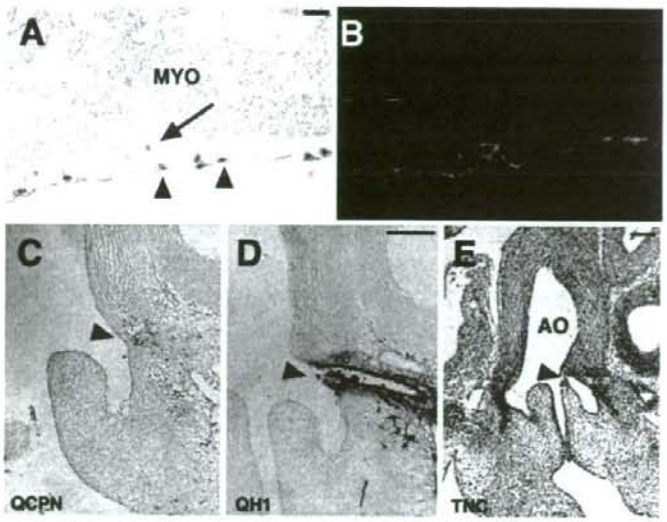

Fig. 3 Expression of tenascin-C in proepidardium chimeras. (A, B) Histological section of the heart doubly immunostained with QCPN and anti-tenascin-C of HH24 (4 days) chimera. Quail-derived epicardial cells (arrowheads) undergo epithelial-mesenchymal transformation (arrow) between the epicardium and myocardium (MYO). Deposition of tenascin-C (green fluorescence) is observed around epithelial-mesenchymal transforming cells (B). (C, D, E) Serial sections of the aorta of HH34 (9 days) chimera immunostained with QCPN (C), QH1 (D), and anti-tenascin-C (TNC) (E). Endothelial cells of the orifice (arrowhead) as well as of the proximal region of coronary artery consist of quail-derived cells. Deposition of tenascin-C can be seen around the proximal region of the coronary artery.
Ao, aorta. Bars in A and D, 50 μm; in E, 100 μm.

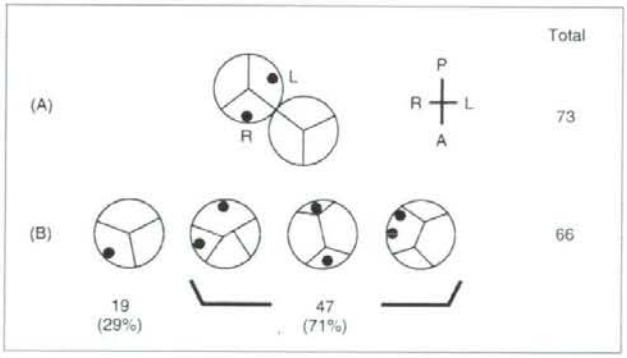

Fig. 4 Anomalies of the coronary orifices of persistent truncus arteriosus in cardiac neural crest-ablated embryos. (A) Schematic presentation of the coronary orifices in control chick embryo. A single coronary orifice is formed at the base of the right (R) and left (L) sinuses of Valsalva of the aortic valve, respectively. (B) Abnormal patterns of valves and coronary orifices in persistent truncus arteriosus at HH36 (10 days). Four valve leaflets are seen in most cases of the truncus arteriosus. A wide variety of coronary orifices, including single coronary and abnormal positioning of two orifices located at various sites, were observed.

左冠動脈弁基部に1個の冠動脈開口が認められた．CNC焼灼除去すると総動脈幹遺残心を作成することができる．66個の総動脈幹遺残を示した心臓では，4弁の総動脈幹弁を示す個体が47例(71%)，3弁は19例(29%)に認められた．3弁の総動脈幹弁では単一の冠動脈開口が観察された．4弁を示す個体では開口部は2個認められるものの，その部位はさまざまであった．これらのことから，CNCは冠動脈開口形成に関与

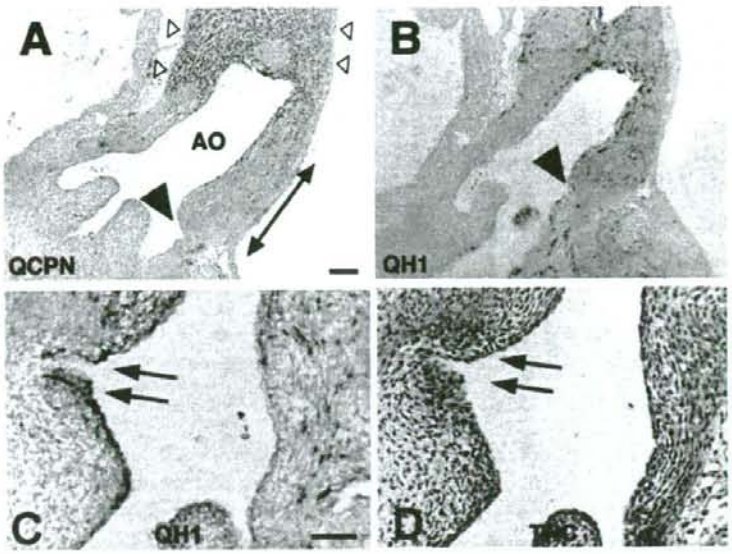

Fig. 5 Distribution of neural crest cells and TNC in the aorta in neural crest chimera.
Serial sagittal sections of HH34 (A, B) and HH30 (C, D) chimera embryo immunostained with QCPN (A), QH1 (B,C) and anti-tenascin-C (TNC) (D). (A) The tunica media of the distal portion of the aorta was consisted of QCPN-positive quail neural crest cells (white arrowheads), whereas QCPN-positive cells were scattered in the proximal wall of the aorta (two-headed arrow). The base of the aorta is suggested to incorporate the cells derived from the secondary heart field. Some of the endothelial cells of the orifice of the coronary artery (arrowhead in B, arrows in C) are QH1 positive. Tenascin-C is expressed around the orifice (arrows in D).
AO, aorta. Scale bar = 50 μm.

している可能性があることが示唆された.

4. 冠動脈開口部形成に関与する細胞とテネイシンC発現

PE移植キメラ胚で, 冠動脈開口部の内皮細胞にPE由来ウズラ細胞が寄与しているのが認められたのは6.5~7日胚HH30~31であった. CNC移植キメラ胚で, 冠動脈開口部を検討したところQCPN抗体では, 大動脈遠位部で多数のウズラ由来CNC陽性細胞が大動脈の中膜平滑筋を形成していた(Fig. 5A, 白色矢頭). 大動脈近位部から大動脈弁まで(両矢印)はCNCウズラ細胞が散在する程度であり, 冠動脈開口部(矢頭)付近では, HNK1抗体によりウズラ細胞が神経節を形成していることを確認した(data not shown). しかし, CNC細胞の冠動脈開口部への明らかな関与は不明であった. QH1抗体で同じ個体を観察したところ, QH1陽性のウズラ細胞数はQCPN陽性細胞に比べて少ないが, 明らかにCNC由来ウズラ細胞が冠動脈開口部および末梢冠動脈内皮の一部を形成しているのを認め(Fig. 5B, C), その周囲にテネイシンCの沈着を認めた(Fig. 5D).

考　察

PEウズラ-ニワトリ移植キメラを使った本研究で, ニワトリ胚心におけるPE由来細胞の時間空間的分布を明らかにした. テネイシンCは冠動脈形成過程で, PE由来細胞が心外膜下でEMTを起こす時期および大動脈基部での冠動脈開口形成時期に特異的に発現しており, 冠動脈形成での重要な役割が示唆された. PE由来細胞は冠動脈平滑筋と内皮細胞, 間質線維芽細胞, さらに心内膜細胞形成に寄与していた. 冠動脈開口部ではPE由来細胞とCNC由来細胞がその形成に関与していた.

1. 心外膜前駆組織由来細胞の分布

3日胚HH19で, PE細胞は心筋に接着後すぐに広がり心外膜形成を開始していた. 4日胚HH24で, 心外膜

下におけるPE由来細胞のEMTがみられたが，これは8日胚まで確認できた．心筋層内に移動するPE由来間葉系細胞は5日胚より認められ，これらは間質線維芽細胞，冠動脈内皮細胞，心内膜細胞へ分化していた．PE由来間葉系細胞は原始血管叢を形成しながら流出路の大動脈基部に向かい，6.5～7日胚HH29～30で大動脈基部血管壁に侵入し，HH30～31で原始冠動脈の大動脈への開口が認められた．

2. 冠動脈開口部を形成する細胞

心外膜は心臓全体を直接被うが，最後に被うのは心臓流出路部分であり，その起源は臓側中胚葉由来の細胞であることが報告されている．心流出路形成は最近の研究によると，二次心臓形成領域(secondary heart field)が関与し流出路で血管平滑筋と心筋の両方に分化するという報告がある[10]．冠動脈開口部は大動脈基部に形成されるが，大動脈血管平滑筋と心筋の中間に位置している．われわれの本研究で，ニワトリ胚のCNC除去により作成した総動脈幹遺残心では，冠動脈開口数の異常を認め，またCNCウズラ-ニワトリキメラ胚で，CNC由来細胞が冠動脈開口部の内皮細胞に寄与していることを見いだした．このことから，PE由来の細胞とCNC細胞の両方が冠動脈開口部を形成していることが明らかとなった．今後，臓側中胚葉由来の細胞が冠動脈開口部に関係しているかどうか検討する必要があると考える．

ニワトリでCNC由来細胞は冠動脈開口部の近位に位置する副交感神経節を形成していることから，冠動脈開口部形成に何らかの働きをしていることが推測されているが[10]，マウスでは神経節は形成されない．CNC細胞に特異的な遺伝子の一つWnt1のトランスジェニックマウスWnt1-creを使ってCNC細胞系譜を追跡することができるが，このマウスの冠動脈の一部にCNC細胞が寄与している[11]．しかし，開口部に関する情報は不明である．CNC細胞に似た動きを示すギャップジャンクションの一つであるコネキシン43の欠損マウスでは冠動脈パターンの異常と単一開口部が認められる[12]．冠動脈開口部にはさまざまな細胞と因子が関わって形成されることが考えられ，ニワトリ胚とマウスを使った比較検討が必要であると考えられる．

3. 心外膜前駆組織由来細胞の制御に関わるテネイシンC

テネイシンCは細胞外基質蛋白の一つであるが，胎児期の器官形成過程で，あたかも形態形成に関わるある種の転写因子のように，一過性に限局した場所に発現するという特徴を有し，特に，細胞遊走に伴って発現がみられることが多い．本研究で，PE由来細胞が心室筋に向かって接着を開始する際にはテネイシンCの強い発現がみられるが，PE細胞が心筋表面に接着すると発現が消失し，心筋表面および心筋層内部へ遊走する際には発現がみられないので，PE由来細胞遊走の制御には直接関わらないと考えられる．また一般に，クッション組織形成などの胎児組織だけでなく，成体組織でも癌浸潤など，EMTに関連して発現が上昇することもよく知られているが，われわれの研究でも，PE由来細胞が心外膜と心筋間でEMTを起こす際に一過性に発現することが明らかになった[13]．EMTは血管形成上極めて重要な段階の一つで，マウスPE組織をコラーゲンゲル層上に培養すると，EMTを起こしてゲルに潜り，内皮細胞や平滑筋細胞に分化して血管様構造を形成するが，コラーゲンコートしたガラス板上に培養してEMTが起きないようにすると血管系細胞に分化しない[13]．つまり，PE由来細胞はEMTにより間葉系細胞になって初めて血管様構造を形成できると考えられることから，in vivoでPE由来細胞がEMTを起こすことは冠動脈形成にとって重要な意味をもつことが推測される．さらに，冠動脈近位部の発達に際し，冠動脈が大動脈へ開口した後でその周囲にテネイシンC発現がみられることから，PE由来細胞あるいはPE由来の原始血管網を大動脈開口予定域に先導するというよりは，大動脈とつながった原始冠動脈壁の成熟に関与すると推測される．

本研究結果とこれまでの文献から得られた情報をFig. 6に示した．房室溝，心室，心房全体を被う心外膜は，横中隔間葉組織から派生するPE細胞由来である．最後に心外膜が被うのは心臓流出路であるが，これには臓側中胚葉由来の細胞も関与していると考えられている(Fig. 6A，C)[6, 14]．発生初期の神経管背側に形成される神経堤細胞のなかで，耳板中央から体節3までの領域(特に，CNCといわれる)細胞が心臓流出路に侵入して流出路中隔を形成する(Fig. 6A，C)．心外膜と心筋との間である心外膜下層では，テネイシンCの発現が多く認められるが，この領域はPE由来細胞がEMTを起こし毛細血管網も多数認められる(Fig. 6B)．この心外膜下層では，VEGF，FGF，PDGF，TGFβなどのシグナルが働いている[10, 14]．冠動脈開口部形成には，PE由来細胞とCNC由来細胞が関わることが判明し，これら細胞周囲にはテネイシンC発現が認められる(Fig. 6D)．冠動脈細胞は，遺伝学的にも多様であることが示されている[15]．

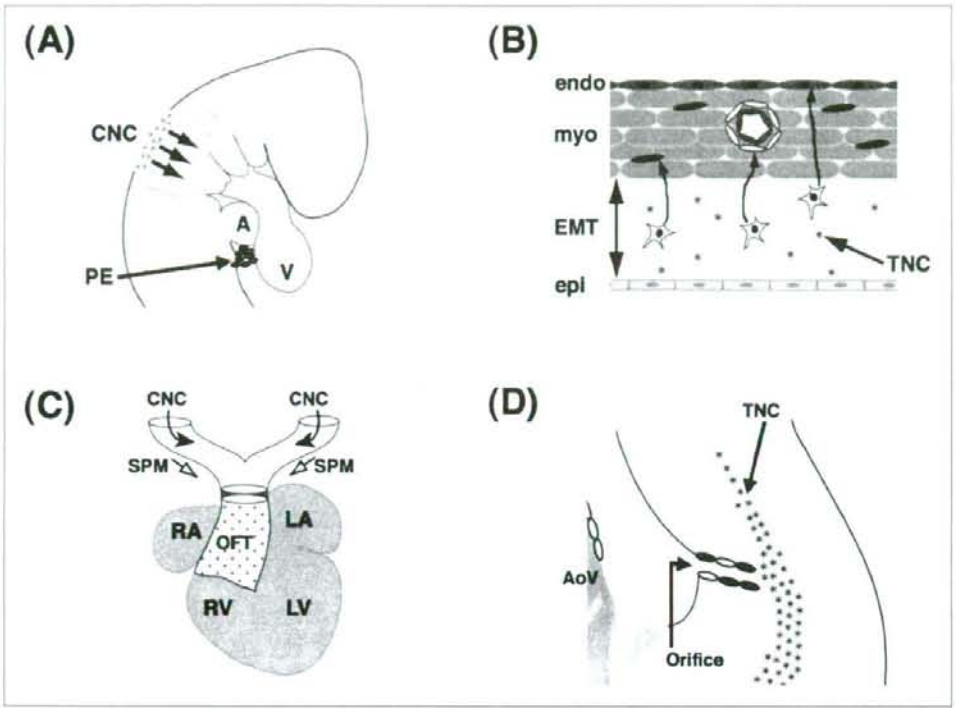

Fig. 6 Spreading, migration and differentiation of epicardium-derived and cardiac neural crest cells.
(A) The proepicardium (PE) derived from the septum transversum between the liver and heart covers most of the atrioventricular junction, ventricles and atria. The cardiac neural crest (CNC) located from the mid-otic placode and somite 3 migrates dorsolaterally through the pharyngeal arches and into the outflow tract of the heart. (B) The epithelial-mesenchymal transformation (EMT) from the epicardium (epi) occurs between the epicardium and myocardium (myo) with deposition of tenascin-C (TNC). The EMT cells differentiate into the endothelium and smooth muscle of the coronary vessels, fibroblasts (blue) and endocardium (endo). (C) The epicardium and splanchnic mesoderm (SPM) cover the outflow tract lastly (dotted area). The CNC migrates into the outflow cushions and is related to the outflow septation. (D) The cells derived from the CNC and PE give rise the coronary orifice. TNC is expressed around the orifice.
A, atrium; AoV, aortic valve; LA, left atrium; LV, left ventricle; OFT, outflow tract; RA, right atrium; RV, right ventricle; V, ventricle

本論文の要旨は第43回日本小児循環器学会総会(2007年7月，東京)で学会長賞を受賞した。

【参考文献】

1) Angelini, P: Coronary artery anomalies: An entity in search of an identity. Circulation 2007; 115: 1296–1305
2) 宮川-富田幸子，今中-吉田恭子，杉村洋子，ほか：冠動脈の発生と発達に関する最近の知見．冠疾患誌 2004；10：55–60
3) Schulte I, Schlueter J, Abu-Issa R, et al: Morphological and molecular left-right asymmetries in the development of the proepicardium: A comparative analysis on mouse and chick embryos. Dev Dyn 2007; 236: 684–695
4) Mikawa T, Gourdie RG: Pericardial mesoderm generates a population of coronary smooth muscle cells migrating into the heart along with ingrowth of the epicardial organ. Dev Biol 1996; 174: 221–232
5) Winter EM, Gittenberger-de Groot AC: Cardiovascular development: Towards biomedical applicability: Epicardium-derived cells in cardiogenesis and cardiac regeneration. Cell Mol Life Sci 2007; 64: 692–703
6) Pérez-Pomares JM, Phelps A, Sedmerova M, et al: Epicardial-like cells on the distal arterial end of the cardiac outflow tract

do not derive from the proepicardium but are derivatives of the cephalic pericardium. Dev Dyn 2003; **227**: 56–68
7. Imanaka-Yoshida K, Matsumoto K, Hara M, et al: The dynamic expression of tenascin-C and tenascin-X during early heart development in the mouse. Differentiation 2003; **71**: 291–298
8. Hasegawa K, Yoshida T, Matsumoto K, et al: Differential expression of tenascin-C and tenascin-X in human astrocytomas. Acta Neuropathol 1997; **93**: 431–437
9. Männer J: Does the subepicardial mesenchyme contribute myocardioblasts to the myocardium of the chick embryo heart? A quail-chick chimera study tracing the fate of the epicardial primordium. Anat Rec 1999; **255**: 212–226
10. Kirby ML: Epicardium and coronary vessel development: Cardiac development. New York, Oxford, 2007, pp133–142
11. Jiang X, Rowitch DH, Soriano P, et al: Fate of the mammalian cardiac neural crest. Development 2000; **127**: 1607–1616
12. Li WE, Waldo K, Linask KL, et al: An essential role for connexin43 gap junctions in mouse coronary artery development. Development 2002; **129**: 2031–2042
13. Watanabe N, Nakagawa M, Hanato T, et al: In vitro model for mouse coronary vasculogenesis. Anat Rec A Discov Mol Cell Evol Biol 2006; **288**: 714–722
14. Wessels A, Pérez-Pomares JM: The epicardium and epicardially derived cells (EPDCs) as cardiac stem cells. Anat Rec A Discov Mol Cell Evol Biol 2004; **276**: 43–57
15. Sun Y, Liang X, Najafi N, et al: Islet 1 is expressed in distinct cardiovascular lineages, including pacemaker and coronary vascular cells. Dev Biol 2007; **304**: 286–296

Journal of Molecular and Cellular Cardiology 46 (2009) 59–66

Contents lists available at ScienceDirect

Journal of Molecular and Cellular Cardiology

journal homepage: www.elsevier.com/locate/yjmcc

Original article

Downregulation of ferritin heavy chain increases labile iron pool, oxidative stress and cell death in cardiomyocytes

Shigemiki Omiya [a], Shungo Hikoso [a], Yukiko Imanishi [b], Atsuhiro Saito [b], Osamu Yamaguchi [a], Toshihiro Takeda [a], Isamu Mizote [a], Takafumi Oka [a], Manabu Taneike [a], Yuko Nakano [c], Yasushi Matsumura [d], Kazuhiko Nishida [a], Yoshiki Sawa [b], Masatsugu Hori [a], Kinya Otsu [a,*]

[a] Department of Cardiovascular Medicine, Osaka University Graduate School of Medicine, 2-2 Yamadaoka, Suita, Osaka 565-0871, Japan
[b] Division of Cardiovascular Surgery, Department of Surgery, Osaka University Graduate School of Medicine, Japan
[c] First Department of Oral and Maxillo-Facial Surgery, Osaka University Graduate School of Dentistry, Japan
[d] Department of Information Science, Osaka University Graduate School of Medicine, Suita, Osaka, Japan

ARTICLE INFO

Article history:
Received 26 May 2008
Received in revised form 29 September 2008
Accepted 30 September 2008
Available online 19 October 2008

Keywords:
Heart failure
Ferritin
Iron
Oxidative stress
Cardiomyocyte death

ABSTRACT

Ferritin heavy chain (FHC) protein was significantly reduced in murine failing hearts following left coronary ligation or thoracic transverse aortic constriction. The mRNA expression of FHC was not significantly altered in failing hearts, compared to that in control sham-operated hearts. Prussian blue staining revealed spotty iron depositions in myocardial infarct failing hearts. Oxidative stress was enhanced in the myocardial infarct failing hearts, as evidenced by increases in 4-hydroxy-2-nonenal and 8-hydroxy-2′-deoxyguanosine immunoreactivity. To clarify the functional significance of FHC downregulation in hearts, we infected rat neonatal cardiomyocytes with adenoviral vector expressing short hairpin RNA targeted to FHC (Ad-FHC-RNAi). The downregulation of FHC induced a reduction in the viability of cardiomyocytes. The relative number of iron deposition-, 4-hydroxy-2-nonenal- or 8-hydroxy-2′-deoxyguanosine-positive cardiomyocytes was significantly higher in Ad-FHC-RNAi-infected cardiomyocytes than in control vector-infected cardiomyocytes. Treatment of Ad-FHC-RNAi-infected cardiomyocytes with desferrioxamine, an iron chelator, significantly reduced the number of iron, 4-hydroxy-2-nonenal or 8-hydroxy-2′-deoxyguanosine-positive cells, and increased viability. In addition, treatment with N-acetyl cysteine, an antioxidant, significantly reduced the number of 4-hydroxy-2-nonenal- or 8-hydroxy-2′-deoxyguanosine-positive cells. Reduced viability in Ad-FHC-RNAi-infected cardiomyocytes was significantly improved with N-acetyl cysteine treatment. These findings indicate that excessive free iron and the resultant enhanced oxidative stress caused by downregulation of FHC lead to cardiomyocyte death. The decrease in FHC expression in failing hearts may play an important role in the pathogenesis of heart failure.

1. Introduction

Several studies have suggested that the level of reactive oxygen species (ROS) increases in the failing heart. It has been postulated that ROS contribute to the pathophysiology of heart failure by initiating myocyte cell death and directly exerting negative inotropic effects [1,2].

The labile iron pool of mammalian cells has been implicated in cell iron regulation and in the production of intracellular ROS. Iron in heme is necessary for the transport, binding, and release of oxygen, and is essential to organism survival. On the other hand, iron also donates electrons for the generation of superoxide radicals and can participate in the regulation of hydroxyl radicals via the Fenton reaction. An excess of free iron must be detoxified by sequestration in ferritin, the major intracellular iron storage protein [3]. Ferritin is a ubiquitous and highly conserved iron-binding protein in vertebrates, and the cytosolic form consists of 2 subunits, termed ferritin heavy chain (FHC) and light chain (FLC). Ferritin has enzymatic activities, converting Fe(II) to Fe(III) as iron is internalized and sequestered in the ferritin mineral core. This function is an inherent feature of FHC, which has ferroxidase activity [3]. The content of cytoplasmic ferritin is regulated by the translation of FHC and FLC mRNAs in response to an intracellular pool of labile iron [3]. This process is mediated by interaction between RNA binding proteins (iron regulatory protein, IRP) and a region in the 5′ untranslated region of FHC and FLC mRNA, termed the iron responsive element (IRE).

In this study, we here demonstrated that the protein level of FHC is downregulated in murine and rat models of heart failure. Knockdown of FHC in isolated cardiomyocytes resulted in increased iron deposition and oxidative stress, leading to cell death. Our findings support the hypothesis that the down-regulation of FHC contributes to cardiomyocyte cell death, and possibly to the development of heart failure.

* Corresponding author.
E-mail address: kotsu@medone.med.osaka-u.ac.jp (K. Otsu).

0022-2828/$ – see front matter © 2008 Elsevier Inc. All rights reserved.
doi:10.1016/j.yjmcc.2008.09.714

2. Materials and methods

2.1. Animals and in vivo assessment of cardiac functions

This study was carried out under the supervision of the Animal Research Committee in accordance with the Guideline on Animal Experiments of Osaka University and the Japanese Government Animal Protection and Management Law (no. 105). Eight-week-old male C57Bl6/J (WT) mice were subjected to surgery. Ligation of the left coronary artery (LCA), causing myocardial infarction (MI), and thoracic transverse aortic constriction (TAC) were performed as described previously [4]. Eight-week-old male Sprague-Dawley (SD) rats were also subjected to ligation of LCA as previously described [5]. Echocardiography was performed on awake mice or anesthetized rat, using ultra-sonography (SONOS-5500, equipped with a 15-MHz linear transducer, Philips Medical Systems) 4 weeks after MI [6].

2.2. Western blot analysis

Total protein homogenates or cell lysates (10 μg per lane) were subjected to Western blot analysis using antibodies against FHC (Abcam), FLC (Alpha Diagnostics International Inc.), transferrin receptor 1 (TfR 1) (Santa Cruz biotechnology, Inc.) and ferroportin 1 (Fpn 1) (Alpha Diagnostics Int'l. Inc.). Western blots were developed using either the ECL Plus kit or the ECL Advance kit (Amersham Biosciences Corp.).

2.3. Quantitative real-time reverse transcriptase-PCR (QRT-PCR) and RNA dot blot analysis

Total RNA was isolated from the left ventricle for analysis using the TRIzol reagent (Life Technologies). The mRNA levels for FHC were determined by quantitative RT-PCR, as previously reported [7]. All data were normalized to GAPDH content and expressed as fold increase over the sham-operated group. Quantitative assessment of FHC or GAPDH mRNA was performed by dot blot analysis, as previously described [7].

2.4. Electrophoretic mobility shift assay (EMSA)

Electrophoretic mobility shift assay (EMSA) was performed using Electrophoretic Mobility Shift Assay kit (Invitrogen Corp.), according to the manufacturer's instructions. The RNA oligonucleotide containing the conserved region of IRE was designed for EMSA as follows: 5'-GUU UCC UGC UUC AAC AGU GCU UGA ACG GAA-3'. Ten μg of total protein homogenates from mouse heart were incubated with 50 ng of RNA oligonucleotides and subjected to electrophoresis on 6% nondenaturing polyacrylamide gels. The gels were stained using SYBR Green EMSA stain and visualized using a FluorImager 595 (Molecular Dynamics) at 488 nm excitation and 530 nm emission.

2.5. Histological and immunohistochemical analysis

The hearts were excised and immediately fixed in buffered 4% paraformaldehyde (PFA), embedded in paraffin, and sectioned to a thickness of 3 μm. We performed Prussian blue staining using the standard procedure and counted the number of iron-positive cardiomyocytes in an area of 4.1×10^5 μm^2 using a light microscopy of a magnification of ×200 [8]. Six to ten fields per section were counted, and the data were averaged. Immunohistochemistry was performed using the Mouse on Mouse Immunodetection Kit (VECTOR Laboratories, Inc.) with mouse anti-4-hydroxy-2-nonenal (HNE) antibody (Japan Institute for the Control of Aging, Japan) and mouse anti-8-hydroxy-2'-deoxyguanosine (8-OHdG) antibody (Oxis International, Inc.). Sections were counterstained with methyl green. The area and intensity of staining for HNE were blinded to score for semiquantification [9]. Briefly, score 0 is no visible staining, 1 is faint staining, 2 is moderate staining, and 3 is strong staining. Expression intensity of 8-OHdG in the myocardium was scored using a previously reported scoring range [9]. The range was as follows: 0 was no labeling, 1 was <50% area labeling of low intensity, 2 was >50% area labeling with low intensity or <50% area labeling with high intensity, and 3 was >50% area with high intensity. We scored on ten color images per section for either HNE or 8-OHdG staining.

2.6. Neonatal cardiomyocyte culture and adenoviral infection

Rat ventricular myocytes from 1- to 2-day-old Wister rats were prepared and cultured as described previously [10]. A 67 bp short hairpin fragment was inserted into the pSIREN-DNR Vector (BD knockout RNAi systems, Clontech) as described previously [6]. The negative control short hairpin RNA (shRNA) (Ad-ns-RNAi) was constructed using Negative Control Annealed Oligonucleotide (BD knockout RNAi systems, Clontech). Cardiomyocytes were infected with adenoviral vectors expressing shRNA targeted to FHC (Ad-FHC-RNAi) or non-specific shRNA (Ad-ns-RNAi) at a multiplicity of infection of 25, and incubated for an additional 6 days. Cardiomyocytes were treated with 0.5 mM desferrioxamine (DFO), 0.2 mM N-acetyl cysteine (NAC), 1 mM vitamin E (Sigma) or 5 μM EUK-8 (Calbiochem) 4 days after infection of Ad-FHC-RNAi.

2.7. Cell death assay

The viability of rat neonatal cardiomyocytes was assessed by cell titer blue (CTB) assay 6 days after infection of Ad-FHC-RNAi. The CTB assay, which measures the metabolic activity of viable cells, was carried out using Cell Titer Blue reagent (Promega) as described previously [11]. The nuclear morphology was observed with 200 μM Hoechst 33258 as described previously [4].

2.8. Cytological and immunocytochemical analysis

The cells were fixed with 4% PFA and permeabilized in 0.1% Triton X-100 5 to 6 days after infection. Prussian blue staining was performed using standard procedure. The cells were incubated in Perl's solution (1% potassium ferrocyanide/1% HCl) at room temperature for 30 min. The first antibodies used for immunocytochemistry were mouse anti-HNE antibody and mouse anti-8-OHdG antibody. The cells were incubated with biotinylated anti-mouse IgG (H+L) affinity purified rat absorbed, and developed with use of a VECTASTAIN Standard ABC reagent.

2.9. Statistical analysis

Results are shown as mean±SEM. Paired data were evaluated by Student's *t*-test, and a one-way analysis of variance (ANOVA) with the Bonferroni's post hoc test was used for multiple comparisons. A value of $P<0.05$ was considered statistically significant.

3. Results

3.1. Downregulation of ferritin heavy chain in heart failure

We examined the FHC expression level in murine and rat failing hearts following MI. MI was caused by ligation of LCA in WT mice or SD rats. Four weeks after surgery, echocardiographic analysis indicated chamber dilatation and cardiac dysfunction (data not shown) [4]. The protein level of FHC in murine whole heart homogenates was significantly reduced in failing hearts after MI compared with that in the corresponding sham-operated hearts (36.6% of sham-operated hearts, $P<0.05$) (Fig. 1A). We observed a

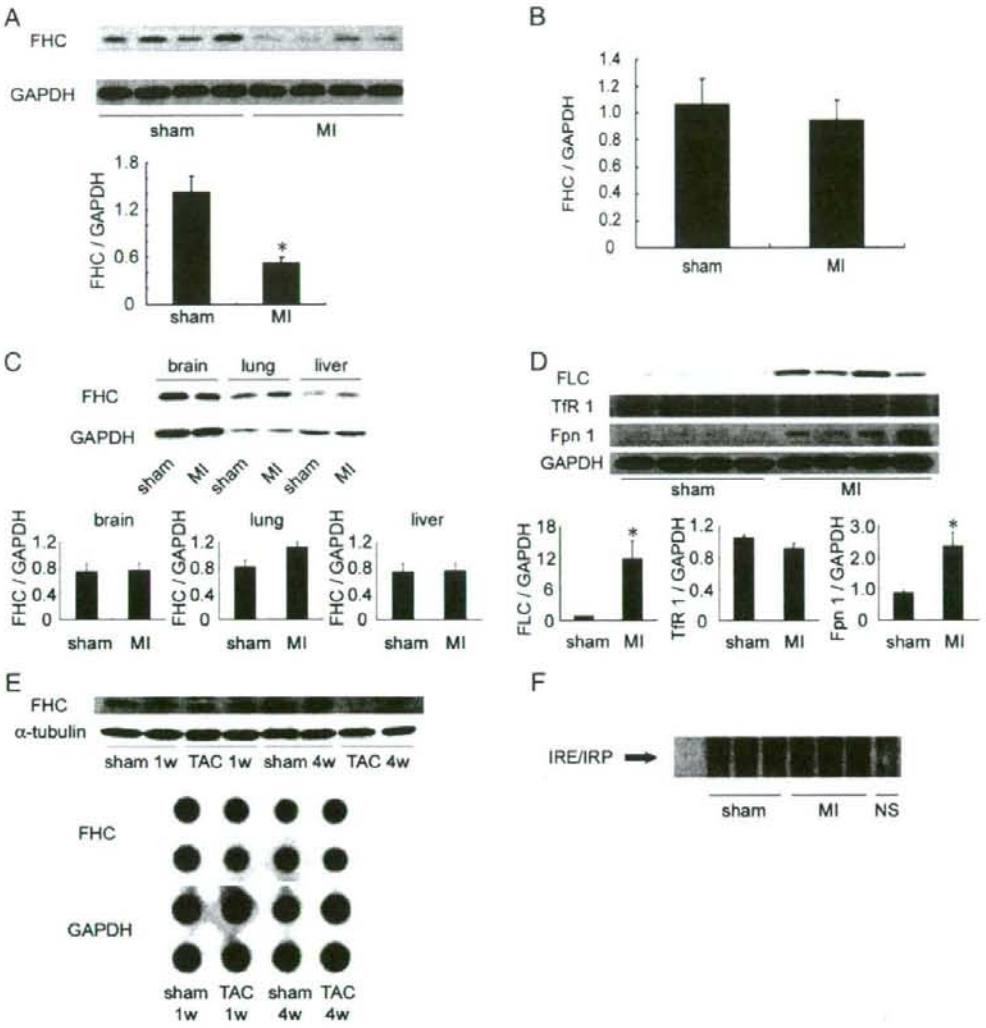

Fig. 1. Ferritin heavy chain (FHC), ferritin light chain (FLC), transferrin receptor 1 (TfR 1) and ferroportin 1 (Fpn 1) expression levels after MI or TAC. (A) FHC protein levels 4 weeks after sham or MI operation in WT hearts were determined by Western blot analysis. GAPDH was used as a protein loading control. Top panels show representative blots, and bottom panel shows signal densities relative to sham-operated controls. Values represent mean ± SEM of data from 5 to 10 mice in each group ($n = 5$ for sham group, $n = 10$ for MI group). *$P < 0.05$ versus sham-operated controls. (B) FHC mRNA levels 4 weeks after sham or MI operation in WT hearts were determined by QRT-PCR analysis. Data were normalized to GAPDH content and are expressed as fold increase over levels in sham-operated controls. Values represent mean ± SEM of data from 4 to 5 mice in each group ($n = 4$ for sham group, $n = 5$ for MI group). (C) FHC protein levels 4 weeks after sham or MI operation in WT brains, lungs, and livers were determined by Western blot analysis. GAPDH was used as a protein loading control. Top panels show representative blots, and bottom panels show signal densities relative to sham-operated controls. Values represent mean ± SEM of data from 3 mice in each group. (D) FLC, TfR 1 and Fpn 1 protein levels 4 weeks after sham or MI operation in WT hearts were determined by Western blot analysis. GAPDH was used as a protein loading control. Top panels show representative blots, and bottom panels show signal densities relative to sham-operated control. Values represent mean ± SEM of data from 4 mice in each group. *$P < 0.05$ versus sham-operated controls. (E) FHC protein levels (upper) and FHC mRNA levels (bottom) 1 to 4 weeks after sham or TAC operation in WT hearts were determined by Western blot analysis and dot blot analysis respectively. α-tubulin protein and GAPDH mRNA were used as a protein loading control. (F) IRP activation in failing hearts. The activation of IRP was analyzed by EMSA. Protein homogenates from mouse heart were incubated with or without RNA oligonucleotides and subjected to electrophoresis. NS represents negative control, which contains no RNA probe.

significant reduction in the FHC protein level in non-infarcted zone of murine MI hearts (54.3% of sham-operated hearts, $P < 0.05$) (Supplemental Figure IA). We normalized the protein level of FHC to that of GAPDH or α-tubulin. These indicate that the downregulation of FHC is not a simple reflection of cell death. In addition, the FHC protein level in rat failing hearts after MI was also significantly reduced compared with that in sham-operated hearts, indicating that the reduction of FHC protein after MI is species-independent (53.8% of sham-operated hearts, $P < 0.05$) (Supplemental Figure IB). On the other hand, QRT-PCR analyses showed that the mRNA expression level of FHC was not significantly different between sham- and MI-operated hearts (Fig. 1B). Furthermore, the protein level of FHC in other organs such as brain, lung and liver showed no significant difference between sham- and MI-operated mice (Fig. 1C).

We next examined FLC, TfR1, the membrane receptor for iron uptake, and Fpn1, the iron exporter. FLC protein was significantly

increased in MI-operated hearts compared with that in the corresponding sham-operated hearts (14.6-fold increase compared with sham-operated hearts) (Fig. 1D). Although TfR1 protein was not significantly different between sham- and MI-operated hearts, Fpn 1 protein was significantly increased in MI-operated hearts compared with that in the corresponding sham-operated hearts (2.7-fold increase compared with sham-operated hearts) (Fig. 1D).

We also examined the FHC expression level in pressure overload-induced failing hearts by means of TAC. The protein level of FHC was significantly reduced in pressure overload-induced failing hearts

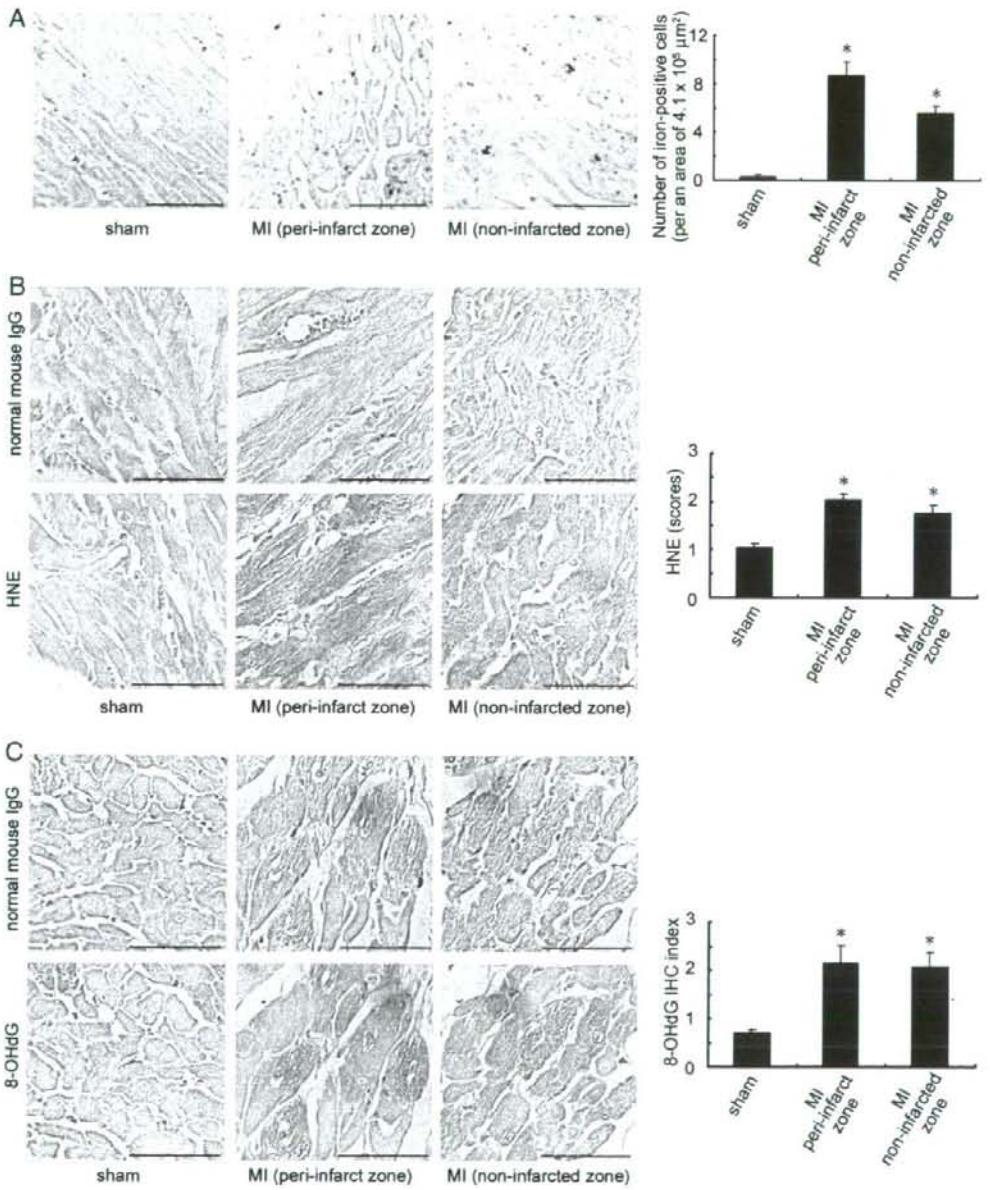

Fig. 2. Histological and immunohistochemical analysis in failing hearts after MI. (A) Histological analysis of iron in failing hearts as assessed by Prussian blue staining. Three panels are sections from sham-operated heart, a peri-infarct zone of MI-operated heart or a non-infarcted zone of MI-operated heart. Bars represent 50 μm. A right graph shows the number of iron-positive cardiomyocytes. Values represent mean ± SEM of data from 3 mice in each group. *$P<0.05$ versus sham-operated hearts. (B and C) Immunohistochemical analysis of oxidative stress assessed by (B) 4-hydroxy-2-nonenal (HNE) and (C) 8-hydroxy-2′-deoxyguanosine (8-OHdG) staining. Normal mouse IgG was used as a negative control. Bars represent 50 μm. In right graphs, the area and intensity were blinded to score for semiquantification (see Materials and method). Values represent mean ± SEM of data from 3 mice in each group. *$P<0.05$ versus sham-operated hearts.

compared with that in the corresponding sham-operated hearts ($P<0.05$) (Fig. 1E). However, dot blot analysis revealed that mRNA expression level of FHC was not significantly different between sham- and TAC-operated failing hearts (Fig. 1E).

To investigate the molecular mechanism underlying the reduction of FHC protein in failing hearts, we evaluated the activation of IRP using EMSA assay. There was no significant difference in IRP activation between sham- and MI-operated hearts (Fig. 1F).

3.2. Cardiac deposition of iron and an increase in oxidative stress in heart failure

Because ferritin plays a key role in maintaining iron homeostasis, the downregulation of FHC may result in the accumulation of free iron in the cytosol [12]. Thus, we assessed the iron deposition in failing hearts after MI by Prussian blue staining (Fig. 2A). The number of iron-positive cardiomyocytes was significantly higher in both peri-infarct and non-infarcted zones in MI-operated hearts compared with that in sham-operated hearts.

Free iron released from FHC induces the generation of ROS through the Fenton/Haber-Weiss reaction [13,14]. We next examined the level of oxidative stress in failing hearts after MI by immunohistochemical staining with anti-HNE or anti-8-OHdG antibodies, oxidative stress markers (Fig. 2B, C). There was a significant increase in HNE immunoreactivity in MI-operated hearts compared with that in sham-operated hearts (Fig. 2B). The increase was observed in both peri-infarct and non-infarcted zones. Myocardial 8-OHdG staining was significantly increased in both peri-infarct and non-infarcted zones in MI-operated hearts compared with that in sham-operated hearts (Fig. 2C).

3.3. Induction of cardiomyocyte death by downregulation of FHC

To clarify the functional significance of FHC downregulation in failing hearts, we infected rat neonatal cardiomyocytes with Ad-FHC-RNAi (Fig. 3A). We constructed three kinds of Ad-FHC-RNAi, called Ad-FHC-RNAi I, II and III. We were able to achieve significant reduction in FHC protein level with Ad-FHC-RNAi I or II 4 days after infection (53.7% and 55.8% of control Ad-ns-RNAi-infected cardiomyocytes, respectively, $P<0.05$) (Fig 3A). Ad-FHC-RNAi III failed to suppress the expression level of FHC. We then examined cardiomyocyte viability 6 days after infection. The viability of cardiomyocytes was significantly reduced in Ad-FHC-RNAi I- or II-infected cardiomyocytes (45.6% and 43.6% of control Ad-ns-RNAi-infected cardiomyocytes, respectively, $P<0.05$). However, there was no significant difference in the viability of Ad-FHC-RNAi III-infected cardiomyocytes compared with that of Ad-ns-RNAi-infected cardiomyocytes (Fig. 3B). To characterize cell death induced by reduction of FHC expression, we examined the nuclear morphology of Ad-FHC-RNAi I- or II-infected cardiomyocytes by staining with Hoechst dye 33258 (Fig. 3C). The number of cardiomyocytes showing nuclear shrinkage, a characteristic feature of necrotic cell death, was significantly increased by infection with Ad-FHC-RNAi I or II [11]. The number of cardiomyocytes showing nuclear fragmentation or chromatin condensation, characteristic features of apoptotic cell death, was not significantly different among cardiomyocytes infected with Ad-FHC-RNAi I, II and Ad-ns-RNAi. These results indicate that the reduction of FHC induced necrotic cardiomyocyte death.

3.4. Contribution of excessive free iron to cardiomyocyte death in FHC-downregulated cardiomyocytes

To clarify the mechanism of cardiomyocyte death induced by the reduction of FHC protein level, we examined whether the downregulation of FHC induces the generation of free iron. We assessed the free iron level in Ad-FHC-RNAi-infected cardiomyocytes by Prussian blue staining (Fig. 4A). Five days after infection, the relative number of iron deposition-positive cardiomyocytes was significantly higher in Ad-FHC-RNAi I- or II-infected cardiomyocytes than that in Ad-ns-RNAi-infected cardiomyocytes. However, treatment with DFO, an iron chelator, significantly reduced the number of iron-positive cells in Ad-FHC-RNAi I or II-infected cardiomyocytes (Fig. 4A). However, RNAi-induced downregulation of FHC did not alter the expression level of Fpn1 in rat neonatal cardiomyocytes (Supplemental Figure II). Next, to examine whether excessive free iron could affect cardiomyocyte

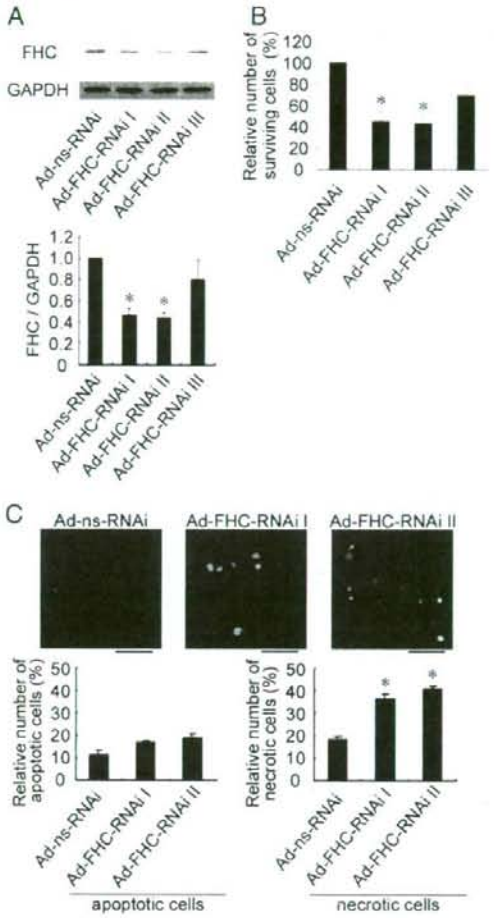

Fig. 3. Cardiomyocyte death by downregulation of FHC. Cardiomyocytes were infected with adenovirus expressing non-specific short hairpin RNA (shRNA) (Ad-ns-RNAi) or three independent shRNA targeted to FHC (Ad-FHC-RNAi I-III). (A) Western blot analysis of FHC in the cardiomyocytes 4 days after infection. Bottom panel shows its densitometric analysis. Values represent mean ± SEM of 3 independent experiments. *$P<0.05$ versus Ad-ns-RNAi-infected cardiomyocytes. (B) Cell viability was assessed by cell titer blue (CTB) assay. Viability of cells is expressed as the percentage of viability of Ad-ns-RNAi-infected cardiomyocytes, when cardiomyocytes were infected with Ad-ns-RNAi or Ad-FHC-RNAi and incubated for 6 days. Values represent mean ± SEM of 3 independent experiments performed in triplicate. *$P<0.05$ versus Ad-ns-RNAi-infected cardiomyocytes. (C) Cardiomyocytes were stained with Hoechst dye 33258 6 days after infection. Upper panels show representative images. Lower panels show relative number of apoptotic or necrotic cells. Values represent mean ± SEM of 3 independent experiments performed in triplicate. *$P<0.05$ versus Ad-ns-RNAi-infected cardiomyocytes. Bars represent 50 μm.

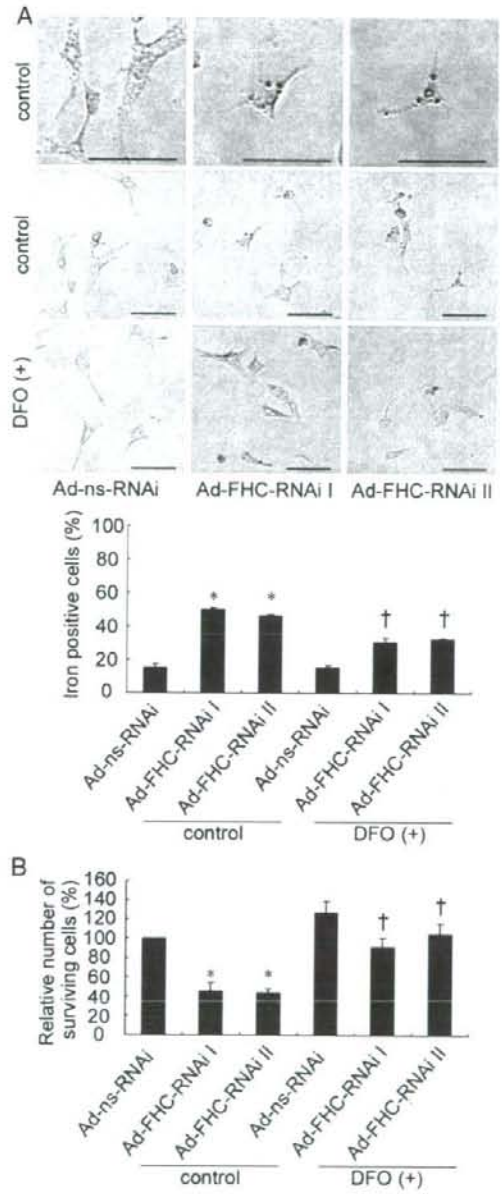

Fig. 4. Iron deposition and cardiomyocyte viability in FHC-downregulated cardiomyocytes. (A) Cytological analysis of iron in FHC-downregulated cardiomyocytes as assessed by Prussian blue staining. Upper panels show representative images of Ad-ns-RNAi-infected or Ad-FHC-RNAi-infected cardiomyocytes stained with Prussian blue staining 5 days after infection. Lower panel shows the percentage of iron positive cells. Bars represent 50 μm. (B) Cardiomyocyte viability was assessed by CTB assay. Viability of cardiomyocytes is expressed as the percentage of viability of Ad-ns-RNAi-infected cardiomyocytes, when cardiomyocytes were infected with Ad-ns-RNAi or Ad-FHC-RNAi and incubated for 6 days. Values represent mean ± SEM of 3 independent experiments performed in triplicate. *$P<0.05$ versus Ad-ns-RNAi-infected cardiomyocytes in control group. †$P<0.05$ versus corresponding control group.

viability, we investigated the effect of DFO on the viability of Ad-FHC-RNAi-infected cardiomyocytes. Reduced viability in Ad-FHC-RNAi I- or II-infected cardiomyocytes was significantly improved with DFO treatment (Fig. 4B).

3.5. Involvement of oxidative stress in FHC downregulation-induced cardiomyocyte death

To examine whether downregulation of FHC induces oxidative stress, we assessed the level of oxidative stress in cardiomyocytes 6 days after infection using immunocytochemical staining with anti-HNE or anti-8-OHdG antibodies. The relative numbers of HNE- or 8-OHdG-positive cardiomyocytes had significantly increased in cardiomyocytes infected with Ad-FHC-RNAi-I or II compared with those in Ad-ns-RNAi-infected cardiomyocytes (Fig. 5A, B). Treatment with NAC, an antioxidant, significantly reduced the number of HNE- or 8-OHdG-positive cells in Ad-FHC-RNAi-I- or II-infected cardiomyocytes. Importantly, chelation of free iron with DFO significantly decreased HNE- or 8-OHdG-positive cardiomyocytes in Ad-FHC-RNAi-I or II-infected cardiomyocytes (Fig. 5A, B). In order to investigate whether the enhanced oxidative stress could affect cardiomyocyte viability, we then examined the effect of NAC on the viability of Ad-FHC-RNAi-infected cardiomyocytes. Reduced viability in Ad-FHC-RNAi-I- or II-infected cardiomyocytes was significantly improved with NAC treatment (Fig. 5C). We also examined the effects of other antioxidants such as vitamin E or EUK-8 on FHC downregulation-induced cardiomyocyte death. Reduced viability in Ad-FHC-RNAi-I- or II-infected cardiomyocytes was significantly improved with vitamin E (Fig. 5D) or EUK-8 (data not shown) treatment.

4. Discussion

The study presented here showed that the protein level of FHC is downregulated in failing hearts after LCA ligation or pressure overload. Thus, it appears that decreased FHC expression is a common feature in failing hearts. Upregulation of Fpn1 compensates for the excess of iron induced by downregulation of FHC in failing hearts.

Ferritin has a large capacity for iron storage and serves to sequestrate and detoxify excess iron. Ferritin is consisted of FHC and FLC, and only FHC has ferroxidase activity. Thus, FHC is more important than FLC to detoxify the harmful function of iron. Ferritin functions to limit Fe(II) available to participate in the generation of ROS. In this study, reducing the expression of FHC by the use of RNAi resulted in increases in iron deposition and oxidative stress. The iron chelator, DFO, inhibited increase in oxidative stress induced by the reduction of FHC in cardiomyocytes. These findings suggest that the reduction of FHC protein expression leads to an increase in labile iron and thereby results in an increase in oxidative stress. Furthermore, DFO, NAC, vitamin E and EUK-8 attenuated cell death induced by the reduction of FHC expression. DFO chelates free iron. NAC is a membrane-permeable precursor of glutathione. EUK-8 is a synthetic superoxide dismutase and catalase mimic [15] and is effective in the prevention of ROS-induced cardiomyocyte death [16]. Vitamin E functions as a lipophilic membrane antioxidant. Iron catalyzes the generation of superoxide radicals and participates in Fenton reaction leading to formation of hydroxyl radicals [3]. The fact that different antioxidants with different modes and sites of action are all effective in the prevention of cardiomyocyte death by the reduction of FHC clearly indicates the involvement of oxidative stress in the mechanism of the death. Thus, reduction of FHC leads to cell death, mediated through increases in labile iron and oxidative stress.

We observed decreased protein levels of FHC, increased levels of iron deposition and oxidative stress in failing hearts. The increased oxidative stress leads to cardiomyocyte cell death and may play an

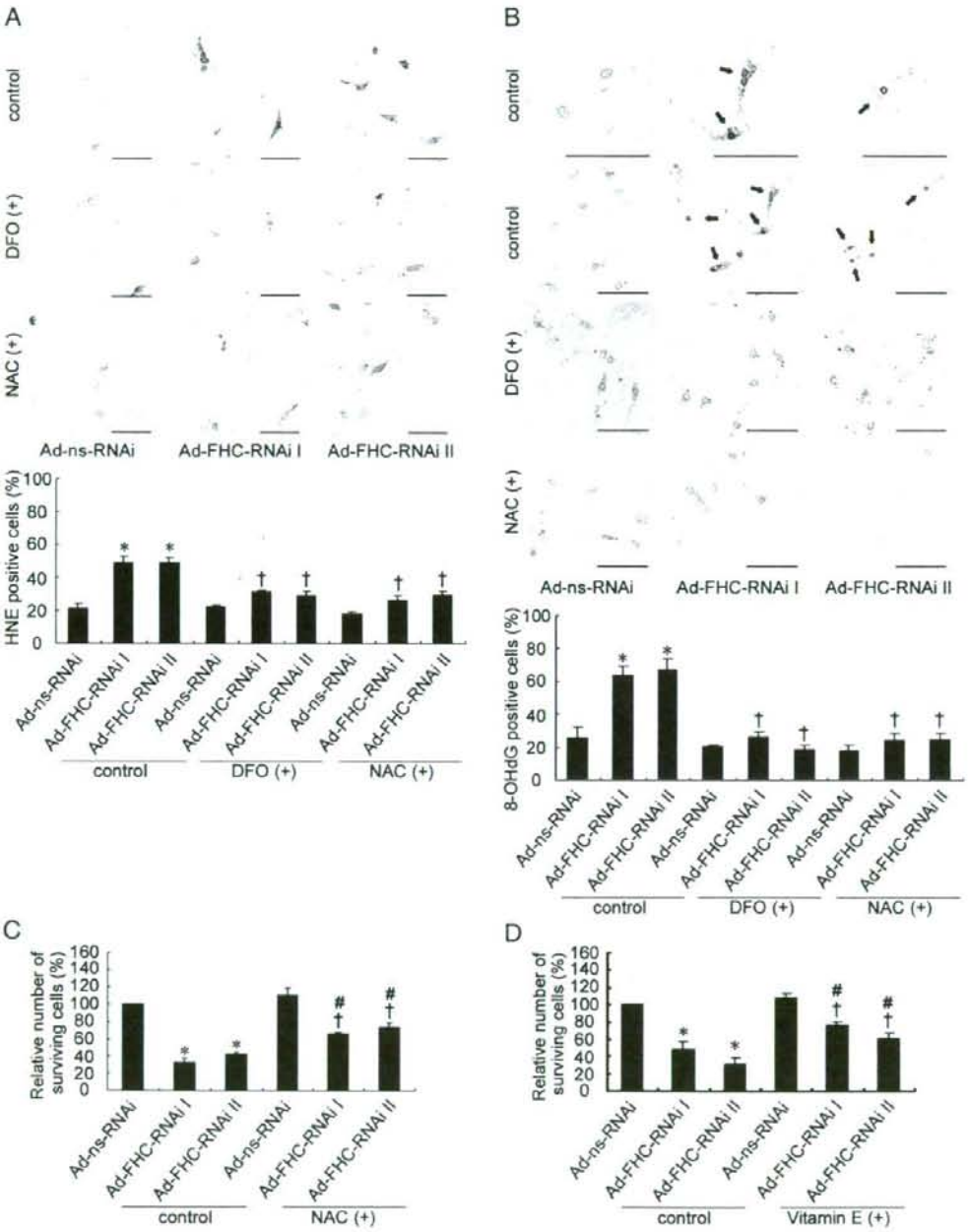

Fig. 5. Oxidative stress and cardiomyocyte viability in FHC-downregulated cardiomyocytes. (A and B) Cytological analysis of oxidative stress in FHC-downregulated cardiomyocytes as assessed by (A) HNE and (B) 8-OHdG staining. (A) Upper panels show representative images of Ad-ns-RNAi- or Ad-FHC-RNAi-infected cardiomyocytes with the treatment of vehicle (control), desferrioxamine (DFO) or N-acetyl cysteine (NAC) stained with HNE 6 days after infection. Bars represent 50 μm. Lower panel shows the percentage of HNE-positive cells. (B) Upper panels show representative images of Ad-ns-RNAi- or Ad-FHC-RNAi-infected cardiomyocytes with the treatment of vehicle (control), desferrioxamine (DFO) or N-acetyl cysteine (NAC) stained with 8-OHdG 6 days after infection. The top three panels are images of control cardiomyocytes at higher magnification. Arrows indicate 8-OHdG-positive cardiomyocytes. Bars represent 50 μm. Lower panel shows the percentage of 8-OHdG-positive cells. (C and D) Cardiomyocyte viability was assessed by CTB assay. Viability of cardiomyocytes is expressed as the percentage of viability of Ad-ns-RNAi-infected cardiomyocytes, when cardiomyocytes were infected with Ad-ns-RNAi or Ad-FHC-RNAi and incubated for 6 days. The effects of treatment with (C) NAC or (D) vitamin E were examined. Values represent mean ± SEM of 3 to 5 independent experiments performed in triplicate ($n=3$ for A–C and $n=5$ for D). $^{*}P<0.05$ versus Ad-ns-RNAi-infected cardiomyocytes in control group. $^{\dagger}P<0.05$ versus corresponding control group. $^{\#}P<0.05$ versus Ad-ns-RNAi-infected cardiomyocytes treated with NAC or vitamin E.

important role in the pathogenesis of heart failure [2]. Although we do not have direct evidence, the decreased level of expression of FHC observed in failing hearts may be involved in the increase in oxidative stress and the pathogenesis of heart failure. Furthermore, there is strong experimental support for ferritin as a protectant against oxidative stress. Exposure to heme induced ferritin synthesis and reduced the cytotoxic response to hydrogen peroxide in endothelial cells and in tumor cell lines [17,18], and overexpression of ferritin reduced ROS levels in cells challenged with hydrogen peroxide and reduced oxidant toxicity [19]. Thus, the decreased expression of FHC in failing hearts leads not only to induced oxidative stress, but also to increased oxidant toxicity.

The protein level of FHC is regulated by both transcriptional and posttranscriptional mechanisms. The transcription of FHC is induced in response to cytokines, hormones, growth factors and second messengers [3]. The translation of ferritin is controlled by the interaction of IRP and IRE. Cytokines also regulate ferritin posttranscriptionally. The induction of ferritin by IL-1β is mediated by protein binding to a region of the mRNA distinct from the IRE [3]. We observed no differences in FHC mRNA expression level between MI- or TAC-induced failing hearts and controls, suggesting that FHC is downregulated through a post-transcriptional mechanism. We did not observe changes in the activation of IRP in failing hearts compared to that in the control non-failing hearts. Furthermore, we showed that FHC was down-regulated, while FLC was upregulated in failing hearts. These findings indicate that the posttranscriptional regulation dependent on the IRP-IRE interaction does not appear to be involved in the downregulation of FHC in failing hearts. Differential degradation of FHC and FLC has been reported in lens epithelial cells, which results in accumulation of L-chain-rich ferritin [20]. It has been reported that oxidized ferritin is degradated by the proteasomal system [21,22]. Oxidation reduces a half-time of both FHC and FLC and this results in a decreased ferritin pool due to oxidative stress. The proteasomal system may be involved in the differential alteration of FHC and FLC protein levels. The molecular mechanism that explains the selective downregulation of FHC in failing hearts remains to be elucidated.

In summary, we first demonstrated that FHC expression is downregulated in failing heart. The decreased level of FHC can induce oxidative stress and cardiomyocyte cell death. Modulation of FHC might be a therapeutic target for the treatment of patients with heart failure.

Appendix A. Supplementary data

Supplementary data associated with this article can be found, in the online version, at doi:10.1016/j.yjmcc.2008.09.714.

References

[1] Lopez Farre A, Casado S. Heart failure, redox alterations, and endothelial dysfunction. Hypertension 2001;38:1400–5.
[2] Giordano FJ. Oxygen, oxidative stress, hypoxia, and heart failure. J Clin Invest 2005;115:500–8.
[3] Torti FM, Torti SV. Regulation of ferritin genes and protein. Blood 2002;99:3505–16.
[4] Yamaguchi O, Higuchi Y, Hirotani S, Kashiwase K, Nakayama H, Hikoso S, et al. Targeted deletion of apoptosis signal-regulating kinase 1 attenuates left ventricular remodeling. Proc Natl Acad Sci USA 2003;100:15883–8.
[5] Imanishi Y, Saito A, Komoda H, Kitagawa-Sakakida S, Miyagawa S, Kondoh H, et al. Allogenic mesenchymal stem cell transplantation has a therapeutic effect in acute myocardial infarction in rats. J Mol Cell Cardiol 2008;44:662–71.
[6] Nakai A, Yamaguchi O, Takeda T, Higuchi Y, Hikoso S, Taniike M, et al. The role of autophagy in cardiomyocytes in the basal state and in response to hemodynamic stress. Nat Med 2007;13:619–24.
[7] Hikoso S, Yamaguchi O, Higuchi Y, Hirotani S, Takeda T, Kashiwase K, et al. Pressure overload induces cardiac dysfunction and dilation in signal transducer and activator of transcription 6-deficient mice. Circulation 2004;110:2631–7.
[8] Danielisova V, Gottlieb M, Burda J. Iron deposition after transient forebrain ischemia in rat brain. Neurochem Res 2002;27:237–42.
[9] Qin F, Simeone M, Patel R. Inhibition of NADPH oxidase reduces myocardial oxidative stress and apoptosis and improves cardiac function in heart failure after myocardial infarction. Free Radic Biol Med 2007;43:271–81.
[10] Hirotani S, Otsu K, Nishida K, Higuchi Y, Morita T, Nakayama H, et al. Involvement of nuclear factor-kappaB and apoptosis signal-regulating kinase 1 in G-protein-coupled receptor agonist-induced cardiomyocyte hypertrophy. Circulation 2002;105:509–15.
[11] Nakagawa T, Shimizu S, Watanabe T, Yamaguchi O, Otsu K, Yamagata H, et al. Cyclophilin D-dependent mitochondrial permeability transition regulates some necrotic but not apoptotic cell death. Nature 2005;434:652–8.
[12] Kakhlon O, Gruenbaum Y, Cabantchik ZI. Repression of ferritin expression increases the labile iron pool, oxidative stress, and short-term growth of human erythroleukemia cells. Blood 2001;97:2863–71.
[13] Curtin JF, Donovan M, Cotter TG. Regulation and measurement of oxidative stress in apoptosis. J Immunol Methods 2002;265:49–72.
[14] Kruszewski M. Labile iron pool: the main determinant of cellular response to oxidative stress. Mutat Res 2003;531:81–92.
[15] Pucheu S, Boucher F, Sulpice T, Tresallet N, Bonhomme Y, Malfroy B, et al. EUK-8 a synthetic catalytic scavenger of reactive oxygen species protects isolated iron-overloaded rat heart from functional and structural damage induced by ischemia/reperfusion. Cardiovasc Drugs Ther 1996;10:331–9.
[16] Pimentel DR, Amin JK, Xiao L, Miller T, Viereck J, Oliver-Krasinski J, et al. Reactive oxygen species mediate amplitude-dependent hypertrophic and apoptotic responses to mechanical stretch in cardiac myocytes. Circ Res 2001;89:453–60.
[17] Balla G, Jacob HS, Balla J, Rosenberg M, Nath K, Apple F, et al. Ferritin: a cytoprotective antioxidant strategem of endothelium. J Biol Chem 1992;267:18148–53.
[18] Cermak J, Balla J, Jacob HS, Balla G, Enright H, Nath K, et al. Tumor cell heme uptake induces ferritin synthesis resulting in altered oxidant sensitivity: possible role in chemotherapy efficacy. Cancer Res 1993;53:5308–13.
[19] Orino K, Lehman L, Tsuji Y, Ayaki H, Torti SV, Torti FM. Ferritin and the response to oxidative stress. Biochem J 2001;357:241–7.
[20] Goralska M, Nagar S, Fleisher LN, McGahan MC. Differential degradation of ferritin H- and L-chains: accumulation of L-chain-rich ferritin in lens epithelial cells. Invest Ophthalmol Vis Sci 2005;46:3521–9.
[21] Mehlhase J, Sandig G, Pantopoulos K, Grune T. Oxidation-induced ferritin turnover in microglial cells: role of proteasome. Free Radic Biol Med 2005;38:276–85.
[22] Shringarpure R, Grune T, Mehlhase J, Davies KJ. Ubiquitin conjugation is not required for the degradation of oxidized proteins by proteasome. J Biol Chem 2003;278:311–8.

European Journal of Heart Failure Advance Access published January 16, 2009

European Journal of Heart Failure
doi:10.1093/eurjhf/hfn049

Suppression of inflammation in rat autoimmune myocarditis by S100A8/A9 through modulation of the proinflammatory cytokine network

Kaoru Otsuka[1], Fumio Terasaki[1]*, Masaki Ikemoto[2], Shuichi Fujita[1], Bin Tsukada[1], Takashi Katashima[1], Yumiko Kanzaki[1], Koichi Sohmiya[1], Tatsuji Kono[1], Haruhiro Toko[3], Masatoshi Fujita[2], and Yasushi Kitaura[1]

[1]Department of Internal Medicine III, Osaka Medical College, 2-7 Daigaku-machi, Takatsuki 569-8686, Japan; [2]Human Health Sciences, Kyoto University Graduate School of Medicine, Japan; and [3]Department of Cardiovascular Science and Medicine, Chiba University Graduate School of Medicine, Japan

Received 31 July 2008; revised 11 September 2008; accepted 20 November 2008

Aims S100A8/A9 is expressed in activated monocytes/macrophages and assumed to be heavily involved in the pathogenesis of acute inflammation. Although several studies have asserted that S100A8/A9 has a proinflammatory function, the exact biological function of S100A8/A9 is yet to be described. We examined the anti-inflammatory effects of S100A8/A9 on experimental autoimmune myocarditis (EAM) in rats.

Methods and results Experimental autoimmune myocarditis was induced in Lewis rats by immunization with porcine cardiac myosin. The recombinant (R-) S100A8/A9 was injected intraperitoneally into EAM rats. R-S100A8/A9 attenuated the severity of myocarditis, as evidenced by echocardiographic and histological findings. In addition, we found that not only the mRNA expression of proinflammatory cytokines [interleukin (IL)-1β, IL-6, and tumour necrosis factor (TNF)-α] in the myocardium, but also their serum concentrations were suppressed in EAM rats treated with R-S100A8/A9. Nuclear factor-kappa B expression in inflammatory cells was also suppressed in the treated rats. To elucidate the mechanistic function of S100A8/A9 on proinflammatory cytokines *in vivo*, we used an ELISA on the supernatant of homogenized heart tissue treated with R-S100A8/A9. The findings revealed high-affinity binding of R-S100A8/A9 with IL-1β, IL-6, and TNF-α in the myocardium, suggesting the trapping of proinflammatory cytokines by R-S100A8/A9.

Conclusion S100A8/A9 attenuates EAM through modulation of the proinflammatory cytokine network.

Keywords S100A8/A9 • Autoimmune myocarditis • Cytokines • Inflammation

Introduction

S100A8/A9, consisting of two low molecular mass subunits (10.6 and 13.5 kDa), is a member of the S100 family and contains two calcium-binding sites per molecule.[1,2] The two subunits are expressed in activated human granulocytes and macrophages in the inflammatory process.[2,3] In activated human neutrophils and macrophages, S100A8 and S100A9 are non-covalently associated to rapidly form the heterodimer S100A8/A9 in a calcium-dependent manner.[2-4] Translocation of the heterodimer from cytoplasm to membrane is induced in the presence of increased intracellular calcium concentration and correlates with the inflammatory action of activated granulocytes and/or macrophages. This protein is known to be involved in several infections and immune diseases, including advanced arthritis, transplant rejection, and sarcoidosis,[5-7] suggesting that it plays an important role in the pathogenesis of the inflammatory process. Although several studies have suggested that S100A8/A9 has a proinflammatory function, we recently demonstrated that S100A8/A9 indirectly suppresses the overproduction of nitrous oxide in activated neutrophils and/or macrophages in rats with lipopolysaccharide-induced liver injury and revealed the binding of S100A8/A9 with proinflammatory

* Corresponding author. Tel: +81 72 683 1221, Fax: +81 72 684 6598, Email: m3012@poh.osaka-med.ac.jp

cytokines *in vitro*.[8] However, the presence of the S100A8/A9-proinflammatory cytokine complexes was not confirmed *in vivo* in that study.

Experimental autoimmune myocarditis (EAM) in rat models is characterized by severe myocardial damage with inflammatory cell infiltration. The EAM model has been widely used as a disease model of human myocarditis,[9] and experimental data have documented that macrophages play a pivotal role in the inflammatory process of EAM in rats.[10]

To verify our hypothesis that S100A8/A9 has an anti-inflammatory effect and to clarify the mechanistic function of S100A8/A9 on proinflammatory cytokines *in vivo*, we treated the EAM rat model with newly prepared recombinant S100A8/A9.

Methods

Preparation of recombinant S100A8/A9

Expression of cDNA for S100A8 or S100A9 in *Escherichia coli* cells

cDNAs with the histidine tag sequence for the human S100A8 and S100A9 subunits were synthesized using PCR.[11] The resulting cDNAs were inserted into pCold I vectors (Takara Bio, Shiga, Japan). The two different expression vectors were then separately transfected into *E. coli* cells. The S100A8 or S100A9 cDNA-transfected *E. coli* cells were cultivated in Miller's LB Broth for 3 h at 37°C. When the absorbance of the culture medium at 600 nm ranged between 0.5 and 0.8, the culture bottle was quickly cooled to 15°C and cultivated for 24 h after adding a final concentration of 1 mmol/L IPTG. The cultivated cells were harvested and then frozen at −80°C until use.

Purification of S100A8 and S100A9 by Ni-agarose affinity column

The *E. coli* cells expressing S100A8 or S100A9 were suspended in 200 mL of binding buffer and then treated by an ultrasonic generator for 10 min at 4°C. After centrifugation at 17 400 *g* for 20 min at 4°C, the supernatant obtained was applied to a Ni-agarose affinity column equilibrated with the binding buffer. After washing the column with washing buffer, S100A8 and S100A9 were eluted from the column with the elution buffer. The fractions containing S100A8 or S100A9 were concentrated to an adequate volume using an Amicon Ultra centrifugal filter device (MW 5000; Millipore, Billerica, MA, USA), and their protein concentrations were obtained by measuring absorbance at 280 nm.

Synthesis and purification of S100A8/A9

Equal molar concentrations of S100A8 and S100A9 were mixed and the mixture was poured into an MW 5000 and incubated overnight in 2.0 mol/L Tris–NaOH solution (pH 12.0) at 4°C. It was dialyzed against 0.1 M Tris–HCl buffer (pH 10.0) containing 300 mM NaCl for 3–4 h at 4°C. After confirming the protein band of recombinant S100A8/A9 by SDS–PAGE, S100A8/A9 was partially purified on a gel filtration column (Sephacryl S-300 HR). Major fractions containing S100A8/A9 were pooled and concentrated to an adequate volume using the same filter device. The above procedures were repeated until the product was adequately concentrated.

Animals and immunization

Animal experimental protocols were approved by the Institutional Animal Care and Use Committee, Osaka Medical College. Male Lewis rats (7 weeks old; body weight 200–250 g) were purchased from Japan SLC (Shizuoka, Japan). Before initiating the experiments, they were kept in cavity for 1 week with free access to food and water. The rats were immunized subcutaneously twice with 0.7 mg purified porcine cardiac myosin (Sigma Chemical Co., St Louis, MO, USA) in an equal volume of complete Freund's adjuvant supplemented with *Mycobacterium tuberculosis* H37RA (Difco, Sparks, MD, USA) on Days 0 and 7.[12]

Administration of recombinant S100A8/A9

Immunized rats were randomly assigned to two groups: Group S (recombinant S100A8/A9, $n = 20$) and Group C (saline as vehicle, $n = 20$). Recombinant S100A8/A9 (1 mg/day) or saline was injected intraperitoneally into the immunized rats each day from Days 8 to 13. On Day 14 or 21, 10 rats in each group (S_{14}, S_{21}, C_{14}, and C_{21}) were sacrificed under ether anaesthesia. Rats that were neither immunized nor received S100A8/A9 were used as normal controls (N_{14} and N_{21}, $n = 5$, respectively).

Echocardiography

Rats were lightly anaesthetized with pentobarbital sodium (1 mg/kg body weight i.p.) on Day 14 or 21. Echocardiography was performed with an echocardiographic apparatus equipped with a 10-MHz transducer (Vivid Five, General Electric-Vingmed, Milwaukee, WI, USA). Two-dimensional targeted M-mode echocardiograms were obtained along the short axis of the left ventricle at the level of the papillary muscles. Left ventricular dimensions at end-diastole (LVDd) and end-systole (LVDs) were measured. Left ventricular ejection fraction (LVEF) was calculated as follows: $[(LVDd^3 - LVDs^3)/LVDd^3] \times 100$.

Histological assessment

For the microscopic evaluation, apex, mid-ventricular, and basal level slices were stained with haematoxylin–eosin. The entire heart and the regions affected by myocarditis (i.e. regions showing inflammation with inflammatory cells and myocardial necrosis) were examined as described previously,[10,13,14] using a computer-assisted analyzer (Scion Image Beta 4.03; Scion Corp, Frederick, MD, USA). The area ratio (percentage value of affected area/entire area) was calculated by two investigators (Y.K. and T.K.) who were blinded to slide identification; the inter- and intra-observer variance was <5%.

Immunohistochemistry

Anti-human S100A8/A9 (rabbit) antibody[6] was used to determine the localization of endogenous S100A8/A9 in Group C_{14}, with anti-rabbit immunogloblins/FITC swine polyclonal antibody (Dako, Denmark) as secondary antibody. Mouse monoclonal antibodies against CD68 were used as a marker for macrophages (AbD serotec, Raleigh, NC, USA), with labelled goat anti-mouse IgG antibody (10 μg/mL, Invitrogen, Carlsbad, CA, USA) as secondary antibody. The resulting fluorescent signal was detected by a fluorescence microscopy.

Rabbit monoclonal antibodies against nuclear factor-kappa B (NF-κB) p65 (Cell Signaling Technology, Danvers, MA, USA) were used to evaluate the activation of NF-κB. The primary antibodies were reacted to sections and immunoreactivity was evaluated using the avidin–biotin horseradish peroxidase complex method (ScyTek Laboratories, Logan, UT, USA). The reactions were optimized with diaminobenzidine chromogen.

Measurement of mRNA levels for proinflammatory cytokines in the heart

RNA isolation and cDNA preparation

RNA was extracted from the excised LV using the RNeasy Mini Kit (Qiagen). The concentration and purity of RNA was determined by measuring the optical density at 260 and 280 nm prior to use. Total RNA (1 μg) from each sample was used for reverse transcription. First strand cDNA was synthesized with random primers and Moloney murine leukaemia virus reverse transcriptase (SuperScript III; Invitrogen).

Quantitative RT–PCR analysis

Quantitative RT–PCR analysis was performed using the LightCycler Real-Time PCR System (Roche Molecular Biochemicals, Indianapolis, IN, USA) to detect the mRNA expression of interleukin (IL)-1β, IL-6, and tumour necrosis factor (TNF)-α. The expression of glyceraldehyde phosphate dehydrogenase (GAPDH) mRNA was measured as the internal control. Assays were designed using the Roche Universal Probe Library (https://www.roche-applied-science.com/sis/rtpcr/upl/index.jsp). For each reaction, the LightCycler Taqman Master Kit (Roche Molecular Biochemicals) was used according to the manufacturer's instructions. PCR cycling was conducted under the following conditions: preheating for 1 cycle at 95 °C for 10 min, amplification for 45 cycles at 95 °C for 10 s and 60 °C for 25 s, and final cooling to 40 °C. mRNA levels were quantified and normalized against levels of GAPDH. The averaged and normalized levels of mRNA in each control group were expressed as 1.0.

Measurement for serum concentrations of proinflammatory cytokines

Serum concentrations of IL-1β, IL-6, and TNF-α were determined by enzyme-linked immunosorbent assay (ELISA) kit (R&D systems, Minneapolis, MN, USA) according to the manufacturer's instructions.

Detection of S100A8/A9–proinflammatory cytokine complexes in heart tissue

The S100A8/A9–proinflammatory cytokine complexes were detected as follows: Heart tissue from EAM rats treated with recombinant S100A8/A9 (Group S_{14}) was quickly homogenized after sacrifice and centrifuged at 7700 *g* at 4 °C. Supernatant was assayed by ELISA in which anti-S100A8/A9 monoclonal antibody was used as the first antibody. S100A8/A9 of the complexes reacted first to the antibody. Subsequently, biotinylated anti-rat IL-1β, IL-6, and TNF-α IgGs were added to the wells and incubated for 1 h at room temperature. After washing with washing buffer, 100 μL of diluted streptavidin–horseradish peroxidase conjugate was added and further incubated for 30 min at room temperature. After washing, colour development of the plate was achieved by adding 100 μL of colour reagent (30 mg o-PD/10 μL of 30% hydrogen peroxide/20 mL of citrate buffer, pH 5.0), and terminated by adding 100 μL of 0.75 mol/L sulfuric acid. The concentrations of the S100A8/A9–IL-1β, IL-6, and TNF-α complexes were obtained using a standard curve for S100A8/A9.

Statistical analysis

Data are expressed as the mean ± SE for continuous variables and as numbers (%) for categorical variables. Multiple comparisons among three groups were performed by ANOVA followed by Scheffe's test (SPSS; Chicago, IL, USA). A *P*-value of <0.05 was considered statistically significant.

Results

Infiltration of macrophages and S100A8/A9

We examined the localization of endogenous S100A8/A9 in the inflamed myocardium of EAM rats by a double staining method using the fluorescent immunohistochemistry. Most of the infiltrating mononuclear cells were positive for CD68, and all cells positive for S100A8/A9 were positive for CD68 (*Figure 1*).

Purification of recombinant S100A8/A9

Recombinant S100A8/A9 was purified successfully. As determined by densitometry, the purity of recombinant S100A8/A9 was ~93% protein concentration (*Figure 2*). The recombinant S100A8/A9 was used in the subsequent study.

Effect of treatment with recombinant S100A8/A9 on the severity of myocarditis

Group S_{14} vs. Group C_{14}

On macroscopic observation, the hearts in Group C_{14} were enlarged and contained large, dark-blue–greyish areas with massive pericardial effusion. The hearts in Group S_{14}, however, were slightly enlarged, had small, dark-blue–greyish areas, and showed almost no pericardial effusion. Echocardiography revealed that LVEF in Group S_{14} was significantly higher than that in Group C_{14} (81 ± 2% vs. 70 ± 3%, $P = 0.017$) (*Figure 3A* and *B*). There was no significant difference in LVEF between Groups N_{14} and S_{14} (85 ± 2% vs. 81 ± 2%). The heart weight (1.02 ± 0.03 g vs. 1.21 ± 0.06 g, $P = 0.015$) as well as the heart weight/body

Figure 1 Infiltration of macrophages and endogenous S100A8/A9 in cardiac tissue of rats with EAM. Most of the infiltrating mononuclear cells were positive for CD68, and all cells positive for S100A8/A9 were positive for CD68 (merged). Bar indicates 25 μm.